Serum Metabolomics Reveals Irreversible Inhibition of Fatty Acid β-Oxidation through the Suppression of PPARα Activation as a Contributing Mechanism of Acetaminophen-Induced Hepato…

ARTICLE *in* CHEMICAL RESEARCH IN TOXICOLOGY · APRIL 2009

Impact Factor: 3.53 · DOI: 10.1021/tx800464q · Source: PubMed

5 AUTHORS, INCLUDING:

Chi Chen
University of Minnesota Twin Cities
73 PUBLICATIONS **3,971** CITATIONS
SEE PROFILE

Yatrik M Shah
University of Michigan
70 PUBLICATIONS **2,542** CITATIONS
SEE PROFILE

Published in final edited form as:
Chem Res Toxicol. 2009 April ; 22(4): 699–707. doi:10.1021/tx800464q.

Serum Metabolomics Reveals Irreversible Inhibition of Fatty Acid β-oxidation through the Suppression of PPARα Activation as a Contributing Mechanism of Acetaminophen-induced Hepatotoxicity

Chi Chen[†,§], **Kristopher W. Krausz**[†], **Yatrik M. Shah**[†], **Jeffrey R. Idle**[‡], and **Frank J. Gonzalez**[†,*]

†*Laboratory of Metabolism, Center for Cancer Research, National Cancer Institute, National Institutes of Health, Bethesda, MD*

‡*Institute of Pharmacology, 1st Faculty of Medicine, Charles University, Prague, Czech Republic*

Abstract

Metabolic bioactivation, glutathione depletion and covalent binding are the early hallmark events after acetaminophen (APAP) overdose. However, the subsequent metabolic consequences contributing to APAP-induced hepatic necrosis and apoptosis have not been fully elucidated. In this study, serum metabolomes of control and APAP-treated wild-type and *Cyp2e1*-null mice were examined by liquid chromatography-mass spectrometry (LC-MS) and multivariate data analysis. A dose-response study showed that the accumulation of long-chain acylcarnitines in serum contributes to the separation of wild-type mice undergoing APAP-induced hepatotoxicity from other mouse groups in a multivariate model. This observation, in conjunction with the increase of triglycerides and free fatty acids in the serum of APAP-treated wild-type mice, suggested that APAP treatment can disrupt fatty acid β-oxidation. A time course study further indicated that both wild-type and *Cyp2e1*-null mice had their serum acylcarnitine levels markedly elevated within the early hours of APAP treatment. While remaining high in wild-type mice, serum acylcarnitine levels gradually returned to normal in *Cyp2e1*-null mice at the end of the 24 h treatment. Distinct from serum aminotransferase activity and hepatic glutathione levels, the pattern of serum acylcarnitine accumulation suggested that acylcarnitines can function as complementary biomarkers for monitoring the APAP-induced hepatotoxicity. An essential role for peroxisome proliferator-activated receptor α (PPARα) in the regulation of serum acylcarnitine levels was established by comparing the metabolomic responses of wild-type and *Ppara*-null mice to a fasting challenge. The upregulation of PPARα activity following APAP treatment was transient in wild-type mice, but was much more prolonged in *Cyp2e1*-null mice. Overall, serum metabolomics of APAP-induced hepatotoxicity revealed that the CYP2E1-mediated metabolic activation and oxidative stress following APAP treatment can cause irreversible inhibition of fatty acid oxidation, potentially through suppression of PPARα-regulated pathways.

*__Correspondence:__ Frank J. Gonzalez, Laboratory of Metabolism, National Cancer Institute, 37 Convent Drive, Bethesda, MD 20892, Tel: 301-402-9067, Fax: 301-496-8419, Email: E-mail: fjgonz@helix.nih.gov.
§Current address: Department of Food Science and Nutrition, University of Minnesota, St. Paul, MN

Supporting Information Available This information is available free of charge via the Internet at http://pubs.acs.org.

Keywords

Acylcarnitine; APAP; β-oxidation; PPARα; CYP2E1; metabolomics; metabolism; LC-MS; hepatotoxicity

Introduction

Acetaminophen (APAP)-induced hepatotoxicity is an important toxicological model for investigating drug-induced liver injury (1). Through saturating glucuronidation and sulfation pathways and depleting thiol antioxidants, APAP overdose overwhelms the intracellular detoxication system. Subsequently, the excessive reactive electrophiles and free radicals originated from cytochrome P450-mediated oxidation of APAP, such as *N*-acetyl-*p*-benzoquinone imine (NAPQI) and hydrogen peroxide, attack the macromolecules in the mitochondria, cell membrane and nuclei, and disrupt the signalling pathways related to cell death and survival, resulting in massive necrosis and apoptosis of hepatocytes (2). Although preclinical studies using cell and animal models and clinical studies on humans undertaken over the past 30 years have provided multifaceted insights into the mechanism of this toxic insult, many unresolved issues remain to be explored. Previous efforts to define the role and importance of several APAP-associated events, such as covalent binding, oxidative stress, the disruption of mitochondrial respiratory chain and membrane structure as well as the autoimmune response, were hampered by the lack of appropriate tools to investigate the APAP-induced molecular events on a global scale. However, recent development in systems biology has provided the technical platform to re-examine APAP-induced hepatotoxicity. For example, genomic and proteomic studies have revealed novel biomarkers of APAP toxicity (3). As for determining the metabolic events induced by APAP, metabolomics provides a new venue to examine the flux of small molecules through a combination of advanced analytical instrumentation and chemometric computation (4,5). NMR-based metabolomics has been adopted to uncover the general changes caused by the APAP-elicited disruption of carbohydrate and lipid metabolism (6,7), while a capillary electrophoresis-MS-based study identified ophthalmic acid as a biomarker of oxidative stress following the APAP-induced glutathione depletion (8). In addition, a recent study on APAP metabolism using an LC-MS-based metabolomics approach identified and characterized novel APAP metabolites associated with the APAP-induced toxicity (9).

Among several APAP-metabolizing cytochromes P450 (P450s), including CYP1A2, CYP2A6, CYP2E1 and CYP3A, CYP2E1 is generally recognized as the major enzyme responsible for the bioactivation of APAP based on enzyme kinetics and properties of APAP intoxication (10,11). This conclusion is further supported by the fact that *Cyp2e1*-null mice are highly resistant to APAP compared to wild-type mice (12) while the reintroduction of the human *CYP2E1* gene into *Cyp2e1*-null mice restores the toxic response to APAP (13). Therefore, *Cyp2e1*-null mouse line can be an ideal negative control for investigating the mechanism and biomarkers of APAP-induced toxicity. In this study, the influences of APAP treatment on the chemical composition of serum from wild-type and *Cyp2e1*-null mice were compared by LC-MS-based metabolomic analysis. Biomarkers originated from the APAP-induced disruption of fatty acid metabolism were further characterized.

Experimental Procedures

Reagents and animals

APAP, palmitoylcarnitine, myristoylcarnitine, glutathione, HPLC-grade water, acetonitrile and formic acid were purchased from Sigma-Aldrich (St. Louis, MO). [$^2H_3$]Palmitoylcarnitine was purchased from Cambridge Isotope Laboratories (Andover, MA).

The *Cyp2e1*-null (*Cyp2e1*-/-) and *Ppara*-null (*Ppara*-/-) mouse lines on the 129/Sv strain background were described previously (12,14). Female wild-type (*Cyp2e1*+/+) and *Cyp2e1*-null mice as well as male wild-type (*Ppara*+/+) and *Ppara*-null mice, from 2 to 3 months of age, were used in this study. All animals were maintained in an NCI animal facility under a standard 12 h light/12 h dark cycle with food and water *ad libitum*. Handling and treatment procedures were in accordance with animal study protocols approved by the NCI Animal Care and Use Committee.

Sample collection

For APAP treatment, APAP was dissolved in a saline solution and administered by intraperitoneal (i.p.) injection at doses of 200 and 400 mg/kg. Control mice were treated with blank saline solution. Serum samples were collected by retro-orbital bleeding at 0.5, 1, 2, 4, 8, 16 and 24 h after APAP treatment. For the fasting experiment, mouse chow was removed from wild-type and *Ppara*-/- mice for 24 h while control mice were still maintained under normal feeding. Serum samples were collected by retro-orbital bleeding at 24 h from both fed and fasted mice. After CO_2 euthanization, liver and other tissue samples were harvested. All samples were stored at -80 °C before analysis.

UPLC-QTOFMS analysis of serum

Deproteinization of serum was conducted by mixing one volume of serum with 20 volumes of 66% aqueous acetonitrile. After a 10-min centrifugation at 18,000 × *g*, a 5 μL aliquot of diluted serum samples was injected into a Waters UPLC-QTOFMS system (Mildford, MA). An Acquity UPLC™ BEH C18 column (Waters) was used to separate chemical components in serum at 35°C. The mobile phase flow rate was 0.5 mL/min with an aqueous acetonitrile gradient containing 0.1% formic acid over a 10-min run. The QTOF Premier™ mass spectrometer was operated in the positive electrospray ionization (ESI) mode. Capillary voltage and cone voltage was maintained at 3 kV and 20 V, respectively. Source temperature and desolvation temperature were set at 120 °C and 350 °C, respectively. Nitrogen was used as both cone gas (50 L/h) and desolvation gas (600 L/h), and argon as collision gas. For accurate mass measurement, the QTOFMS was calibrated with sodium formate solution (range *m*/*z* 100-1000) and monitored by the intermittent injection of the lock mass sulfadimethoxine ($[M+H]^+$ = 311.0814 *m*/*z*) in real time. Mass chromatograms and mass spectral data were acquired and processed by MassLynx software (Waters) in centroided format. The structures of serum biomarkers were elucidated by tandem MS (MS^2) fragmentation with collision energies ranging from 15 to 30 eV.

Multivariate data analysis (MDA)

Chromatographic and spectral data of serum samples were deconvoluted by MarkerLynx™ software (Waters). A multivariate data matrix containing information on sample identity, ion identity (RT and *m*/*z*) and ion abundance was generated through centroiding, deisotoping, filtering, peak recognition and integration. The intensity of each ion was calculated by normalizing the single ion counts (SIC) *versus* the total ion counts (TIC) in the whole chromatogram. The data matrix was further exported into SIMCA-P+™ software (Umetrics, Kinnelon, NJ), and transformed by mean-centering and *Pareto* scaling, a technique that increases the importance of low abundance ions without significant amplification of noise. Based on the complexity and quality of the data, either unsupervised or supervised MDA were adopted to analyze the serum data from untreated/treated wild-type and *Cyp2e1*-null mice as well as from fed/starved wild-type and *Ppara*-null mice. Major latent variables in the data matrix were described in a scores scatter plot of multivariate model. Potential biomarkers were identified by analyzing ions contributing to the principal components and to the separation of sample groups in the loadings scatter plot.

Quantitation of palmitoylcarnitine in serum

Deproteinated serum samples from wild-type and *Cyp2e1*-null mice were analyzed by use of an API 2000™ mass spectrometer (Applied Biosystems, Foster City, CA). Deuterated palmitoylcarnitine ([$^2H_3$]Palmitoylcarnitine) was used as internal standard. Samples were injected into a high-performance liquid chromatography (HPLC) system (PerkinElmer, Waltham, MA) using a Luna C18 column (Phenomenex, Torrance, CA, 50 × 2.1 mm i.d.). The flow rate through the column at ambient temperature was 0.3 mL/min with a gradient (methanol: water: acetonitrile, containing 0.1% formic acid) from 5: 60: 35 to 5: 5: 90 in a 6-min run. The column was equilibrated for 1.5 min before each injection. The mass spectrometer was operated in the turbo ion spray mode with positive ion detection; the turbo ion spray temperature was maintained at 350°C, and a voltage of 4.5 kV was applied to the sprayer needle. Nitrogen was used as the turbo ion spray and nebulizing gas. Detection and quantification were performed using the multiple reactions monitoring mode, with *m*/*z* 400.3/85.0 for palmitoylcarnitine and *m*/*z* 403.3/85.0 for [$^2H_3$]palmitoylcarnitine. Using Analyst software (Applied Biosystems), serum palmitoylcarnitine concentrations were determined by calculating the ratio between the peak area of palmitoylcarnitine and the peak area of [$^2H_3$] palmitoylcarnitine and fitting with a calibration curve with a linear range from 10 nM to 1 μM (r = 0.99).

Quantitation of hepatic glutathione

The levels of reduced glutathione (GSH) in liver were measured by LC-MS/MS. Samples for GSH measurement were prepared by homogenizing liver in 10 volumes of 5% 5-sulfosalicylic acid. Precipitated protein was removed by centrifugation at 10,000 × *g* for 10 minutes and supernatant was diluted by deionized water prior to LC-MS analysis. Samples were injected into a high-performance liquid chromatography (HPLC) system (PerkinElmer) using a Synergi Polar-RP column (Phenomenex, 50 × 2.1 mm i.d.). The flow rate through the column at ambient temperature was 0.2 mL/min with a gradient (methanol: water: acetonitrile, containing 0.1% formic acid) from 5: 85: 10 to 5: 40: 55 in a 5-min run. The column was equilibrated for 1.5 min before each injection. API 2000™ mass spectrometer (Applied Biosystems) was operated in the turbo ion spray mode with positive ion detection. The turbo ion spray temperature was maintained at 350°C, and a voltage of 5.5 kV was applied to the sprayer needle. Nitrogen was used as the turbo ion spray and nebulizing gas. Detection and quantification were performed using the multiple reactions monitoring mode, with *m*/*z* 308.0/75.9 for GSH.

Assessment of APAP-induced toxicity

APAP-induced liver injury was evaluated by measuring the catalytic activities of asparate aminotransferase (AST) in serum. Briefly, 1 μL serum was mixed with 200 μL AST assay buffer (Catachem, Bridgeport, CT) in a 96-well microplate, and the oxidation of NADH to NAD^+ was monitored at 340 nm for 5 minutes.

Assessment of the influence of APAP treatment on fatty acid metabolism

APAP-induced disruption of fatty acid metabolism was evaluated by measuring the levels of serum triglycerides and free fatty acids using colorimetric triglyceride assay reagent (Thermo Electron, Noble Park, Australia) and free fatty acid assay reagent (Wako, Osaka, Japan), respectively.

RNA analysis

Total RNA was extracted from the livers of wild-type and *Cyp2e1*-null mice using TRIzol reagent (Invitrogen, Carlsbad, CA). Quantitative real-time PCR (qPCR) was performed using cDNA generated from 1 mg total RNA with SuperScript III Reverse Transcriptase kit (Invitrogen). Primers were designed using the Primer Express software (Applied Biosystems)

and sequences are enlisted in Supplemental Table 1. qPCR reactions were carried out using SYBR green PCR master mix (Superarray, Frederick, MD) using an ABI Prism 7900HT Sequence Detection System (Applied Biosystems). Gene expression levels were quantified using the Comparative CT method, and normalized to 18S rRNA.

Statistics

Experimental values are expressed as mean ± standard deviation (SD). Statistical analysis was performed with two-tailed Student's *t*-tests for unpaired data, with a p value of <0.05 was considered as statistically significant.

Results

Serum metabolomics of dose-dependent response to APAP treatment

Liver is the main target of APAP-induced toxicity. Serum, as the major deposit of metabolites generated in the liver, was used as the source for metabolomic analysis. Results from previous studies have shown that wild-type mice were susceptible to 400 mg/kg APAP and also mildly affected by 200 mg/kg APAP, while *Cyp2e1*-null mice were highly resistant to both doses (9,12). To explore the mechanism underlying the different responses to APAP treatments between wild-type and *Cyp2e1*-null mice, serum metabolomes of two mouse lines were analyzed by a UPLC-QTOFMS system and characterized by MDA. The data set of each sample was the summation of ions detected by LC-MS system while each ion was represented by retention time (RT), mass/charge ratio (*m/z*) and ion counts. Data extracted from the chromatograms and mass spectra of serum samples were processed by a partial least squares-discriminant analysis (PLS-DA), a supervised MDA method. A two-component model was further constructed to delineate the relationship among sample groups as well as the contribution of each detected serum chemical ion to the principal components (PC) of the multivariate model (5). Sample distribution pattern in the scores scatter plot indicated that 24-h serum samples from the 200 mg/kg treatment of wild-type and *Cyp2e1*-null mice and the 400 mg/kg treatment of *Cyp2e1*-null mice were mainly separated from the untreated wild-type and *Cyp2e1*-null mice in the second component (PC2) of the model (Figure 1*A*), suggesting that mild changes in the chemical composition of serum still occurred even though the hepatotoxic effect of APAP were minimal in these three mouse groups. More strikingly, the wild-type mice treated with 400 mg/kg APAP were clearly separated from all five mouse groups in the first and most important component (PC1) of the model that largely defines the relationship among samples. The fact that this observation was consistent with the hepatotoxic status of this mouse group implied that the ions contributing to the construction of PC1 might correlate to the APAP-induced liver toxicity, and therefore be potential biomarkers. Analysis of the loadings plot of this model revealed the existence and properties of serum ions that determined the distinctive distribution of the wild-type mice treated with 400 mg/kg APAP (Figure 1*B*). Among them, the chemical identities of four ions (**I**-**IV**) that had the highest correlation with the wild-type mice treated with 400 mg/kg APAP were further elucidated by MS^2 and accurate mass measurements. Interestingly, the fragmentation of four ions with *m/z* of 400.34^+, 372.31^+, 426.35^+ and 398.32^+ all resulted in very similar mass spectra, in which a carnitine fragment (*m/z* = 85.0289^+ of $^+CH_2$-CH=CH-COOH fragment) and fatty acid moiety appeared (Figure 1*C* and Supplemental Figure 1*A*-*C*). Accurate mass measurement of four ions defined their molecular formula as $C_{23}H_{45}NO_4^+$, $C_{21}H_{41}NO_4^+$ $C_{25}H_{47}NO_4^+$ and $C_{23}H_{43}NO_4^+$, corresponding to palmitoylcarnitine (**I**), myristoylcarnitine (**II**), oleoylcarnitine (**III**) and palmitoleoylcarnitine (**IV**), respectively, which are major long-chain acylcarnitine species in serum. Identities of the palmitoylcarnitine and myristoylcarnitine ions were further confirmed by authentic standards. Moreover, the quantitation of palmitoylcarnitine levels in serum confirmed the conclusion of metabolomic analysis (Figure 1*D*). Twenty-four hours after 400 mg/kg APAP treatment, the palmitoylcarnitine level in wild-type mice was about five-fold

higher than the corresponding control. Interestingly, the basal level of palmitoylcarnitine in *Cyp2e1*-null mice was significantly lower than its level in wild-type mice.

Since long-chain acylcarnitines are the essential intermediates of fatty acid β-oxidation in mitochondria and peroxisomes, the changes of serum acylcarnitine levels have been associated with lipid metabolism disorders (15,16). To correlate the acylcarnitine levels with the fatty acid metabolism in wild-type and *Cyp2e1*-null mice, the influence of APAP treatment on the levels of serum triglycerides (TG) and free fatty acids (FFA) was examined. Consistent with the profile of acylcarnitines, the dramatic increases of serum TG and FFA only occurred in the wild-type mice treated with 400 mg/kg APAP while 200 mg/kg APAP significantly decreased the serum TG level in both wild-type and *Cyp2e1*-null mice (Figure 2*A*-*B*). This observation confirmed that APAP overdose can severely disrupt the β-oxidation-related lipid metabolism.

Analysis of the APAP-elicited time-dependent changes in the serum metabolomes of wild-type and Cyp2e1-null mice

Examination of serum samples harvested 24 h after APAP treatment demonstrated a clear correlation between metabolomic profile and hepatotoxicity and revealed the dramatic increase of serum acylcarnitines in the treated wild-type mice exhibiting hepatotoxicity (Figure 1). However, since APAP-induced liver injury is an acute process driven by many crucial events that occur in the early hours of APAP exposure, such as disruption of the mitochondrial outer membrane and depletion of thiol antioxidants (2), the metabolomic changes observed at 24 h could be either the direct consequences of, or the indirect side effects of, APAP-induced hepatotoxicity. To determine the kinetics of APAP-induced changes in the serum metabolomes of wild-type and *Cyp2e1*-null mice, serum samples harvested at 0, 0.5, 1, 2, 4, 8, 16, 24 h after 400 mg/kg APAP treatment were analyzed by UPLC-QTOFMS, and data collected were further processed by principal components analysis (PCA), an unsupervised MDA method. As indicated in the scores plot (Figure 3*A* and Supplemental Figure 2*A*), both the chemical components in the serum metabolomes of wild-type and *Cyp2e1*-null mice changed in a time-dependent manner following APAP treatment. However, the changes that occurred in wild-type mice were far more dramatic than those in *Cyp2e1*-null mice in the dimensions of PC1 and PC2 of the model, leading to a clear post-treatment separation between wild-type and *Cyp2e1*-null mice along PC1 (Figure 3*A* and Supplemental Figure 2*A*). Analysis of the loadings plot further confirmed that palmitoylcarnitine, one of the most abundant acylcarnitines in serum, was still one of major contributors to the PC1 of this PCA model (Supplemental Figure 2*B*). To obtain a temporal view of APAP-induced acylcarnitine accumulation, time-dependent changes in serum palmitoylcarnitine levels were further measured (Figure 3*B*). Although no change occurred at 0.5 h, serum pamitoylcarnitine levels in both mouse lines increased dramatically and reached a comparable level at 1 h of APAP treatment. At 2 h, the increase of serum pamitoylcarnitine in wild-type mice was more dramatic than its increase in *Cyp2e1*-null mice and led to a significant difference between the groups. More strikingly, serum palmitoylcarnitine levels remained high in wild-type mice after 2 h of APAP treatment while its level in *Cyp2e1*-null mice slowly returned to basal levels at the end of 24 h. This result indicated that the homeostasis of acylcarnitines in both mouse lines was significantly affected by 400 mg/kg APAP treatment and the increase of serum palmitoylcarnitine was an early event in the APAP-induced toxicity. In addition, profiling the kinetics of serum palmitoylcarnitine revealed that the APAP-induced influences on serum acylcarnitines were transient in *Cyp2e1*-null mice, but persistent in wild-type mice (Figure 3*B*). To explore the significance of this observation, the pattern of serum palmitoylcarnitine levels was compared with the patterns of serum AST activity and hepatic glutathione levels, two widely used biomarkers of APAP-induced hepatotoxicity (Figure 3*C*-*D*). The results indicated that each of three biomarkers had different profiles in wild-type and *Cyp2e1*-null mice during the 24-h post-APAP period. Compared to serum palmitoylcarnitine, serum AST activity was not affected in *Cyp2e1*-null

mice, and its increase in wild-type mice, which occurred at 2 h, was also behind the increase in serum palmitoylcarnitine, which occurred at 1 h (Figure 3*C*). In contrast to the delayed response in AST activity, hepatic glutathione levels in both mouse lines declined dramatically at 0.5 h of APAP treatment, that preceded the increase of serum palmitoylcarnitine (Figure 3*D*). After maximum depletion at 2 h, hepatic glutathione levels in *Cyp2e1*-null mice quickly recovered at 4 h of APAP treatment. Interestingly, hepatic glutathione levels in wild-type mice had also recovered at 16 h of APAP treatment, which was in contrast to the irreversible acylcarnitine accumulation and fulminating toxic response in wild-type mice (Figure 3*D*). Overall, these results indicated that, compared to the changes of serum aminotransferase and hepatic glutathione levels, the changes in acylcarnitine levels reflects a different facet of the pathophysiological changes induced by APAP overdose.

Acylcarnitine accumulation induced by the fasting challenge to Ppara-null mice

Accumulation of acylcarnitine as well as triglycerides and free fatty acids following 400 mg/kg APAP treatment suggested that APAP overdose can inhibit the β-oxidation of fatty acids, which is the principal catabolic pathway for energy generation when glucose metabolism is blocked or suppressed, such as occurs during fasting. As the central regulator of fatty acid transport and β-oxidation, the nuclear transcriptional factor peroxisome proliferator-activated receptor alpha (PPARα) plays an important role in the adaptive response to fasting (17,18). Therefore, a potential correlation between PPARα function and acylcarnitine accumulation was explored by comparing the metabolomic responses of wild-type and *Ppara*-null mice to a 24-h fasting challenge. Following LC-MS analysis of serum samples from fasted and fed wild-type and *Ppara*-null mice, a two-component PLS-DA model was constructed (Figure 4). The distribution pattern of fed wild-type and *Ppara*-null mice in the model revealed the existence of intrinsic metabolomic differences that were mainly defined by the PC2 of the model. Moreover, the overlapping of fasted wild-type mice with fed wild-type mice in the model suggested that wild-type mice were capable of avoiding major changes in the chemical components of serum metabolome through adjusting energy metabolism pathways, including β-oxidation, to adapt to fasting (Figure 4*A*). In contrast, fasting elicited significant changes in the serum metabolome of *Ppara*-null mice, as shown by a dramatic shift between fed and fasted *Ppara*-null mice in the model (Figure 4*A*). Therefore, serum metabolomics was able to reflect the reported lipid disorder in *Ppara*-null mice following fasting challenge (17,18). More importantly, analysis of the loadings plot of this multivariate model further showed that palmitoylcarnitine (**I**), myristoylcarnitine (**II**), oleoylcarnitine (**III**) and palmitoleoylcarnitine (**IV**) were also important contributors to the separation of starved *Ppara*-null mice from other three mouse groups, thereby suggesting a direct connection between the accumulation of long-chain acylcarnitines and inhibition of PPARα function (Figure 4*B*).

Differential responses of PPARα-targeted genes to APAP treatment in wild-type and Cyp2e1-null mice

Based on the observed relationship between the deficiency of PPARα function and the fasting-elicited acylcarnitine accumulation in *Ppara*-null mice (Figure 4), the correlation of PPARα function and APAP-induced acylcarnitine accumulation in wild-type and *Cyp2e1*-null mice was examined by measuring the expression kinetics of four PPARα target genes, including carnitine palmitoyltransferase 1 (*Cpt1*), carnitine palmitoyltransferase 2 (*Cpt2*), acyl-CoA thioesterase 1 (*Acot1*) and cytochrome P450 4A10 (*Cyp4a10*), in the livers of wild-type and *Cyp2e1*-null mice. The major increase of *Cpt1* gene expression was observed in both wild-type and *Cyp2e1*-null mice at 0.5 h after APAP treatment which is earlier than the acylcarnitine accumulation in serum. However, the high expression level of *Cpt1* was sustained through 24 h only in *Cyp2e1*-null mice while its expression in wild-type mice was gradually reduced to basal level at the end of 24 h (Figure 5*A*). Compared to *Cpt1*, the induction of *Cpt2* in *Cyp2e1*-null mice was much delayed and less intense. Moreover, its expression in wild-type

mice only increased transiently in the first 2 h, and then gradually decreased to less than half of the basal level (Figure 5*B*). Although the expression of *Acot1* in both mouse lines returned to its basal level at 24 h of APAP treatment, the induction of *Acot1* in *Cyp2e1*-null mice was much stronger and more prolonged than its induction in wild-type mice (Figure 5*C*). As for *Cyp4a10*, its expression pattern in the APAP-treated wild-type and *Cyp2e1*-null mice was largely similar to the expression pattern of *Cpt1* (Figure 5*D*). Overall, albeit some differences among four PPARα target gene expression pattern was found, it is clear that PPARα activation in *Cyp2e1*-null mice was much more significant and more persistent than its activation in wild-type mice following high-dose APAP treatment, leading to more prolonged upregulation of PPARα-targeted genes that are involved in the fatty acid β-oxidation pathway.

Discussion

Inhibition of fatty acid β-oxidation has been established as a major mechanism of the hepatotoxicity induced by many therapeutic agents and environmental toxicants, including aspirin and hypoglycin (19). However, inhibition of β-oxidation has not been implicated as a contributing factor in the APAP-induced hepatotoxicity cascade even though it is known that APAP overdose can cause severe disruption of lipid metabolism, such as the occurrence of microvesicular steatosis and increase of triglycerides and free fatty acids (2,20). In this study, through a metabolomic analysis of dose-dependent responses of wild-type and *Cyp2e1*-null mice to APAP treatment, a novel correlation between the susceptibility to APAP and the accumulation of long-chain acylcarnitines (**I-IV**) in serum was identified. This observation suggested that APAP and/or its metabolites can negatively affect fatty acid β-oxidation in the liver since long-chain acylcarnitines are the principal precursors of β-oxidation substrates and the acylcarnitines in serum mainly originate from the liver (21). A time-course study further indicated that fatty acid oxidation might be a primary target, instead of a side effect, of APAP toxicity since the accumulation of acylcarnitines occurred within the first hour of APAP treatment in both wild-type and *Cyp2e1*-null mice, which was earlier than the increase of serum aminotransferase activity. More interestingly, the high levels of serum acylcarnitines were sustained in APAP-sensitive wild-type mice, but gradually reduced to the basal levels in APAP-resistant *Cyp2e1*-null mice at the end of 24-h treatment. This correlation between the resistance to APAP and the acylcarnitine levels in serum implied that the response to early inhibition of β-oxidation might have significant influence on the pathophysiological consequence of APAP overdose. In fact, the observation of acylcarnitine accumulation in this study was consistent with the reported APAP-induced carnitine depletion as the accumulation of acylcarnitines prevents the recycling of free carnitine (22). Moreover, it was shown that both pre-dosing and post-dosing of free carnitine can significantly reduce and relieve the APAP-induced symptoms (22,23), suggesting that the fatty acid oxidation system has a protective effect against APAP-induced toxicity. It is known that mitochondrial proteins are the main targets of APAP-elicited covalent binding (24,25) and APAP overdose inhibits mitochondrial respiration (26) and induces mitochondrial permeability transition (27,28). Therefore, inhibition of fatty acid β-oxidation might be a consequence of APAP-elicited structural damage to mitochondria or a direct effect of inhibiting of enzymes and transporters involving in the β-oxidation pathway by the reactive APAP metabolites and the reactive oxygen species (ROS) generated by CYP2E1-mediated reactions. With regard to the consequence of the inhibition of β-oxidation, it is noteworthy that the acylcarnitine accumulation observed in this study was highly correlated with the reported glycogen depletion in the livers of mice treated with the hepatotoxic doses of APAP (29). Thus, it is reasonable to propose that inhibition of β-oxidation by APAP may trigger or induce activation of the glycogenolysis pathway for maintaining the balance of energy metabolism even though the APAP-induced functional deficiency in the mitochondrial oxidation system may prevent the efficient utilization of released glucose. In fact, this crosstalk between two major pathways of energy generation can potentially explain the fasting-induced susceptibility to APAP since, following APAP and fasting treatments, energy metabolism in

the liver is blocked by both β-oxidation inhibition and glycogen depletion (30). Overall, the dramatic disruption of energy metabolism by CYP2E1-mediated APAP bioactivation plays an important role in APAP-induced hepatotoxicity (31).

The reversible inhibition of β-oxidation in *Cyp2e1*-null mice and irreversible inhibition in wild-type mice, as shown by the time course study on the palmitoylcarnitine level in serum, indicated a reciprocal relationship between serum acylcarnitine levels and APAP resistance. The underlying mechanism was investigated through analysis of the metabolic responses of wild-type and *Ppara*-null mice to the fasting challenge, in which the observation of acylcarnitine accumulation in the fasted *Ppara*-null mice revealed a pivotal role for PPARα in regulating serum acylcarnitine levels. The positive influence of PPARα activation on the resistance to APAP toxicity was suggested by the observation that induction of PPARα-targeted gene expression following APAP treatment was persistent in *Cyp2e1*-null mice, but only transient in wild-type mice. This correlation between PPARα activation and resistance to APAP was also supported by several experimental findings: 1) Besides APAP, exposure to hydrazine, another potent hepatotoxin, also induced the expression of PPARα-targeted genes (32). Therefore, activation of the PPARα pathway might be a common cytoprotective event in response to hepatotoxicity. 2) PPARα activation in streptozotocin-treated wild-type mice contributed to the diabetes-induced resistance to APAP as the resistance was abolished in *Ppara*-null mice. Without PPARα activation, both wild-type and *Ppara*-null mice were susceptible to the high-dose APAP exposure (33). 3) Multiple treatments with PPARα ligands, such as fibrates (clofibrate) and fatty acids (docosahexaenoic acid), dramatically reduced APAP toxicity (34,35). However, the protective effect of ligand treatment was abolished in *Ppara*-null mice (35). More importantly, a single-dose pretreatment of clofibrate also significantly reduced the APAP toxicity without reduction of covalent binding and the decrease of GSH depletion (36). 4) Alcohol treatment induced hepatic steatosis and enhanced APAP toxicity in *Cyp2e1*-null mice (37). Simultaneously, alcohol treatment also profoundly inhibited PPARα function in *Cyp2e1*-null mice (38). All of these observations suggested that the resistance of *Cyp2e1*-null mice to APAP might be partially attributed to the robust activation of PPARα that can reduce the release of surplus acylcarnitines into serum through enhancing fatty acid oxidation processes. Currently, the mechanisms by which the early activation of PPARα signaling was downregulated in wild-type mice following APAP treatment are not clear. However, preliminary data revealed that APAP administration does not result in decreased PPARα protein expression (data not shown). Therefore, the suppression of PPARα activation in wild-type mice might be the results of reduced metabolic capacity for generating energy required for mRNA synthesis, posttranslational modifications of PPARα by altered signal transduction pathways, or a decrease of endogenous PPARα ligands caused by the prolonged oxidative stress. It was shown that PPARα activity is regulated by multiple kinases (39), which could be affected by APAP treatment. In addition, the levels and composition of endogenous PPARα ligands, such as nitrated unsaturated fatty acids (40), could be significantly affected by the APAP-induced redox imbalance and inhibition of nitric oxide synthase (41). Future biochemical, proteomic and lipidomic studies should provide valuable information on these issues.

The levels of long-chain acylcarnitines in serum, including palmitoylcarnitine, have been used as clinical biomarkers for screening inborn genetic defects in fatty acid oxidation pathways (42-44), but their application as biomarkers of APAP-induced hepatotoxicity has not been reported. The results from this study clearly showed that serum palmitoylcarnitine level, especially its kinetic profile, can provide predictive information for monitoring the initiation and progression of APAP-elicited liver injury. Compared to hepatic GSH and serum aminotransferases, two well-established biomarkers of APAP toxicity, palmitoylcarnitine level was more responsive than aminotransferase activity at the early hours after APAP treatment and more indicative than glutathione level at the later times after APAP treatment. Therefore,

palmitoylcarnitine may complement glutathione and aminotransferase for predicting the consequence and prognosis of APAP toxicity and other drug-induced liver injury, although its value as a biomarker still requires clinical validation. In addition, the combination of palmitoylcarnitine with lactate (45) and phosphate (46) levels in serum can function as useful indicators of the status of energy metabolism system. Another interesting observation in this study is the dramatic decrease of hepatic GSH in *Cyp2e1*-null mice during the first 2 h of APAP overdose since it is generally believed that the lack of CYP2E1 function in this knockout mouse should reduce the conversion of APAP to NAPQI, a reaction mainly responsible for the GSH depletion. As shown in a recent study on APAP metabolism (9), this hypothesis is valid for the low-dose and non-hepatotoxic APAP treatment, in which glucuronidation and sulfation, instead of GSH conjugation, are more prominent metabolic pathways in *Cyp2e1*-null mice than in wild-type mice. However, in APAP overdose, the differences between *Cyp2e1*-null and wild-type mice with regard to the formation of GSH, *N*-acetyl cysteine (NAC) and cysteine conjugates of APAP become far less significant. It is very likely that the CYP3As and CYP1A2-mediated bioactivation of APAP contributes to the GSH depletion in *Cyp2e1*-null mice since the high concentrations of APAP in liver during early times after APAP overdose are sufficient for the K_m of CYP3As and CYP1A2, that is higher than CYP2E1.

In summary, by combining genetically-modified mouse model and high-resolution LC-MS, metabolomic analysis of serum samples from APAP-treated wild-type and *Cyp2e1*-null mice identified long-chain acylcarnitines as the early biomarkers of APAP-induced hepatotoxicity, and further revealed that the suppression of PPARα activation may contribute to the sustained inhibition of fatty acid β-oxidation. These results establish the value of LC-MS-based metabolomics and suggest its future application as an efficient tool to investigate the molecular mechanism of toxic events.

Supplementary Material

Refer to Web version on PubMed Central for supplementary material.

Acknowledgements

This study was supported by the NCI Intramural Research Program of the NIH. J.R.I is grateful to US Smokeless Tobacco Company for a grant for collaborative research.

Abbreviations

APAP, acetaminophen
GSH, reduced glutathione
P450, cytochrome P450
AST, aspartate aminotransferase
TG, triglycerides
FFA, free fatty acids
PPARα, peroxisome proliferator-activated receptor alpha
MDA, multivariate data analysis
PCA, principal components analysis
PLS-DA, partial least squares-discriminant analysis
MS^2, tandem mass spectrometry
LC-MS, liquid chromatography-mass spectrometry
UPLC, ultra-performance liquid chromatography
TOFMS, time-of-flight mass spectrometry

References

(1). Larson AM, Polson J, Fontana RJ, Davern TJ, Lalani E, Hynan LS, Reisch JS, Schiodt FV, Ostapowicz G, Shakil AO, Lee WM. Acetaminophen-induced acute liver failure: results of a United States multicenter, prospective study. Hepatology 2005;42:1364–1372. [PubMed: 16317692]

(2). Cohen, SD.; Hoivik, DJ.; Khairallah, EA. Acetaminophen-Induced Hepatotoxicity. In: Plaa, GL.; Hewitt, WR., editors. Toxicology of the Liver. Taylor & Francis; 1998. p. 159-186.

(3). Ruepp SU, Tonge RP, Shaw J, Wallis N, Pognan F. Genomics and proteomics analysis of acetaminophen toxicity in mouse liver. Toxicol Sci 2002;65:135–150. [PubMed: 11752693]

(4). Nicholson JK, Wilson ID. Opinion: understanding `global' systems biology: metabonomics and the continuum of metabolism. Nat Rev Drug Discov 2003;2:668–676. [PubMed: 12904817]

(5). Chen C, Gonzalez FJ, Idle JR. LC-MS-based metabolomics in drug metabolism. Drug Metab Rev 2007;39:581–597. [PubMed: 17786640]

(6). Coen M, Lenz EM, Nicholson JK, Wilson ID, Pognan F, Lindon JC. An integrated metabonomic investigation of acetaminophen toxicity in the mouse using NMR spectroscopy. Chem Res Toxicol 2003;16:295–303. [PubMed: 12641429]

(7). Coen M, Ruepp SU, Lindon JC, Nicholson JK, Pognan F, Lenz EM, Wilson ID. Integrated application of transcriptomics and metabonomics yields new insight into the toxicity due to paracetamol in the mouse. J Pharm Biomed Anal 2004;35:93–105. [PubMed: 15030884]

(8). Soga T, Baran R, Suematsu M, Ueno Y, Ikeda S, Sakurakawa T, Kakazu Y, Ishikawa T, Robert M, Nishioka T, Tomita M. Differential metabolomics reveals ophthalmic acid as an oxidative stress biomarker indicating hepatic glutathione consumption. J Biol Chem 2006;281:16768–16776. [PubMed: 16608839]

(9). Chen C, Krausz KW, Idle JR, Gonzalez FJ. Identification of novel toxicity-associated metabolites by metabolomics and mass isotopomer analysis of acetaminophen metabolism in wild-type and Cyp2e1-null mice. J Biol Chem 2008;283:4543–4559. [PubMed: 18093979]

(10). Patten CJ, Thomas PE, Guy RL, Lee M, Gonzalez FJ, Guengerich FP, Yang CS. Cytochrome P450 enzymes involved in acetaminophen activation by rat and human liver microsomes and their kinetics. Chem Res Toxicol 1993;6:511–518. [PubMed: 8374050]

(11). Lieber CS. Cytochrome P-4502E1: its physiological and pathological role. Physiol Rev 1997;77:517–544. [PubMed: 9114822]

(12). Lee SS, Buters JT, Pineau T, Fernandez-Salguero P, Gonzalez FJ. Role of CYP2E1 in the hepatotoxicity of acetaminophen. J Biol Chem 1996;271:12063–12067. [PubMed: 8662637]

(13). Cheung C, Yu AM, Ward JM, Krausz KW, Akiyama TE, Feigenbaum L, Gonzalez FJ. The cyp2e1-humanized transgenic mouse: role of cyp2e1 in acetaminophen hepatotoxicity. Drug Metab Dispos 2005;33:449–457. [PubMed: 15576447]

(14). Lee SS, Pineau T, Drago J, Lee EJ, Owens JW, Kroetz DL, Fernandez-Salguero PM, Westphal H, Gonzalez FJ. Targeted disruption of the alpha isoform of the peroxisome proliferator-activated receptor gene in mice results in abolishment of the pleiotropic effects of peroxisome proliferators. Mol Cell Biol 1995;15:3012–3022. [PubMed: 7539101]

(15). Foster DW. The role of the carnitine system in human metabolism. Ann N Y Acad Sci 2004;1033:1–16. [PubMed: 15590999]

(16). Pande SV, Murthy MS. Carnitine-acylcarnitine translocase deficiency: implications in human pathology. Biochim Biophys Acta 1994;1226:269–276. [PubMed: 8054358]

(17). Kersten S, Seydoux J, Peters JM, Gonzalez FJ, Desvergne B, Wahli W. Peroxisome proliferator-activated receptor alpha mediates the adaptive response to fasting. J Clin Invest 1999;103:1489–1498. [PubMed: 10359558]

(18). Leone TC, Weinheimer CJ, Kelly DP. A critical role for the peroxisome proliferator-activated receptor alpha (PPARalpha) in the cellular fasting response: the PPARalpha-null mouse as a model of fatty acid oxidation disorders. Proc Natl Acad Sci U S A 1999;96:7473–7478. [PubMed: 10377439]

(19). Fromenty B, Pessayre D. Inhibition of mitochondrial beta-oxidation as a mechanism of hepatotoxicity. Pharmacol Ther 1995;67:101–154. [PubMed: 7494860]

(20). Buttar HS, Nera EA, Downie RH. Serum enzyme activities and hepatic triglyceride levels in acute and subacute acetaminophen-treated rats. Toxicology 1976;6:9–20. [PubMed: 941168]

(21). Sandor A, Cseko J, Kispal G, Alkonyi I. Surplus acylcarnitines in the plasma of starved rats derive from the liver. J Biol Chem 1990;265:22313–22316. [PubMed: 2266127]

(22). Nowaczyk MJ, Whelan D, Hill RE, Clarke JT, Pollitt RJ. Long-chain hydroxydicarboxylic aciduria, carnitine depletion and acetaminophen exposure. J Inherit Metab Dis 2000;23:188–189. [PubMed: 10801061]

(23). Yapar K, Kart A, Karapehlivan M, Atakisi O, Tunca R, Erginsoy S, Citil M. Hepatoprotective effect of L-carnitine against acute acetaminophen toxicity in mice. Exp Toxicol Pathol 2007;59:121–128. [PubMed: 17716880]

(24). Qiu Y, Benet LZ, Burlingame AL. Identification of the hepatic protein targets of reactive metabolites of acetaminophen in vivo in mice using two-dimensional gel electrophoresis and mass spectrometry. J Biol Chem 1998;273:17940–17953. [PubMed: 9651401]

(25). Landin JS, Cohen SD, Khairallah EA. Identification of a 54-kDa mitochondrial acetaminophen-binding protein as aldehyde dehydrogenase. Toxicol Appl Pharmacol 1996;141:299–307. [PubMed: 8917703]

(26). Meyers LL, Beierschmitt WP, Khairallah EA, Cohen SD. Acetaminophen-induced inhibition of hepatic mitochondrial respiration in mice. Toxicol Appl Pharmacol 1988;93:378–387. [PubMed: 3368917]

(27). Masubuchi Y, Suda C, Horie T. Involvement of mitochondrial permeability transition in acetaminophen-induced liver injury in mice. J Hepatol 2005;42:110–116. [PubMed: 15629515]

(28). Reid AB, Kurten RC, McCullough SS, Brock RW, Hinson JA. Mechanisms of acetaminophen-induced hepatotoxicity: role of oxidative stress and mitochondrial permeability transition in freshly isolated mouse hepatocytes. J Pharmacol Exp Ther 2005;312:509–516. [PubMed: 15466245]

(29). Hinson JA, Mays JB, Cameron AM. Acetaminophen-induced hepatic glycogen depletion and hyperglycemia in mice. Biochem Pharmacol 1983;32:1979–1988. [PubMed: 6870927]

(30). Price VF, Miller MG, Jollow DJ. Mechanisms of fasting-induced potentiation of acetaminophen hepatotoxicity in the rat. Biochem Pharmacol 1987;36:427–433. [PubMed: 3827934]

(31). Andersson BS, Rundgren M, Nelson SD, Harder S. N-acetyl-pbenzoquinone imine-induced changes in the energy metabolism in hepatocytes. Chem Biol Interact 1990;75:201–211. [PubMed: 2369786]

(32). Richards VE, Chau B, White MR, McQueen CA. Hepatic gene expression and lipid homeostasis in C57BL/6 mice exposed to hydrazine or acetylhydrazine. Toxicol Sci 2004;82:318–332. [PubMed: 15282401]

(33). Shankar K, Vaidya VS, Corton JC, Bucci TJ, Liu J, Waalkes MP, Mehendale HM. Activation of PPAR-alpha in streptozotocin-induced diabetes is essential for resistance against acetaminophen toxicity. Faseb J 2003;17:1748–1750. [PubMed: 12958197]

(34). Nguyen KA, Carbone JM, Silva VM, Chen C, Hennig GE, Whiteley HE, Manautou JE. The PPAR activator docosahexaenoic acid prevents acetaminophen hepatotoxicity in male CD-1 mice. J Toxicol Environ Health A 1999;58:171–186. [PubMed: 10522648]

(35). Chen C, Hennig GE, Whiteley HE, Corton JC, Manautou JE. Peroxisome proliferator-activated receptor alpha-null mice lack resistance to acetaminophen hepatotoxicity following clofibrate exposure. Toxicol Sci 2000;57:338–344. [PubMed: 11006363]

(36). Manautou JE, Emeigh Hart SG, Khairallah EA, Cohen SD. Protection against acetaminophen hepatotoxicity by a single dose of clofibrate: effects on selective protein arylation and glutathione depletion. Fundam Appl Toxicol 1996;29:229–237. [PubMed: 8742320]

(37). Sinclair JF, Szakacs JG, Wood SG, Walton HS, Bement JL, Gonzalez FJ, Jeffery EH, Wrighton SA, Bement WJ, Sinclair PR. Short-term treatment with alcohols causes hepatic steatosis and enhances acetaminophen hepatotoxicity in Cyp2e1(-/-) mice. Toxicol Appl Pharmacol 2000;168:114–122. [PubMed: 11032766]

(38). Wan YY, Cai Y, Li J, Yuan Q, French B, Gonzalez FJ, French S. Regulation of peroxisome proliferator activated receptor alpha-mediated pathways in alcohol fed cytochrome P450 2E1 deficient mice. Hepatol Res 2001;19:117–130. [PubMed: 11164737]

(39). Burns KA, Vanden Heuvel JP. Modulation of PPAR activity via phosphorylation. Biochim Biophys Acta 2007;1771:952–960. [PubMed: 17560826]

(40). Baker PR, Lin Y, Schopfer FJ, Woodcock SR, Groeger AL, Batthyany C, Sweeney S, Long MH, Iles KE, Baker LM, Branchaud BP, Chen YE, Freeman BA. Fatty acid transduction of nitric oxide signaling: multiple nitrated unsaturated fatty acid derivatives exist in human blood and urine and serve as endogenous peroxisome proliferator-activated receptor ligands. J Biol Chem 2005;280:42464–42475. [PubMed: 16227625]

(41). Godfrey L, Bailey I, Toms NJ, Clarke GD, Kitchen I, Hourani SM. Paracetamol inhibits nitric oxide synthesis in murine spinal cord slices. Eur J Pharmacol 2007;562:68–71. [PubMed: 17331495]

(42). Gempel K, Kiechl S, Hofmann S, Lochmuller H, Kiechl-Kohlendorfer U, Willeit J, Sperl W, Rettinger A, Bieger I, Pongratz D, Gerbitz KD, Bauer MF. Screening for carnitine palmitoyltransferase II deficiency by tandem mass spectrometry. J Inherit Metab Dis 2002;25:17–27. [PubMed: 11999976]

(43). Van Hove JL, Kahler SG, Feezor MD, Ramakrishna JP, Hart P, Treem WR, Shen JJ, Matern D, Millington DS. Acylcarnitines in plasma and blood spots of patients with long-chain 3-hydroxyacyl-coenzyme A dehydrogenase defiency. J Inherit Metab Dis 2000;23:571–582. [PubMed: 11032332]

(44). Rubio-Gozalbo ME, Bakker JA, Waterham HR, Wanders RJ. Carnitine-acylcarnitine translocase deficiency, clinical, biochemical and genetic aspects. Mol Aspects Med 2004;25:521–532. [PubMed: 15363639]

(45). Bernal W, Donaldson N, Wyncoll D, Wendon J. Blood lactate as an early predictor of outcome in paracetamol-induced acute liver failure: a cohort study. Lancet 2002;359:558–563. [PubMed: 11867109]

(46). Schmidt LE, Dalhoff K. Serum phosphate is an early predictor of outcome in severe acetaminophen-induced hepatotoxicity. Hepatology 2002;36:659–665. [PubMed: 12198658]

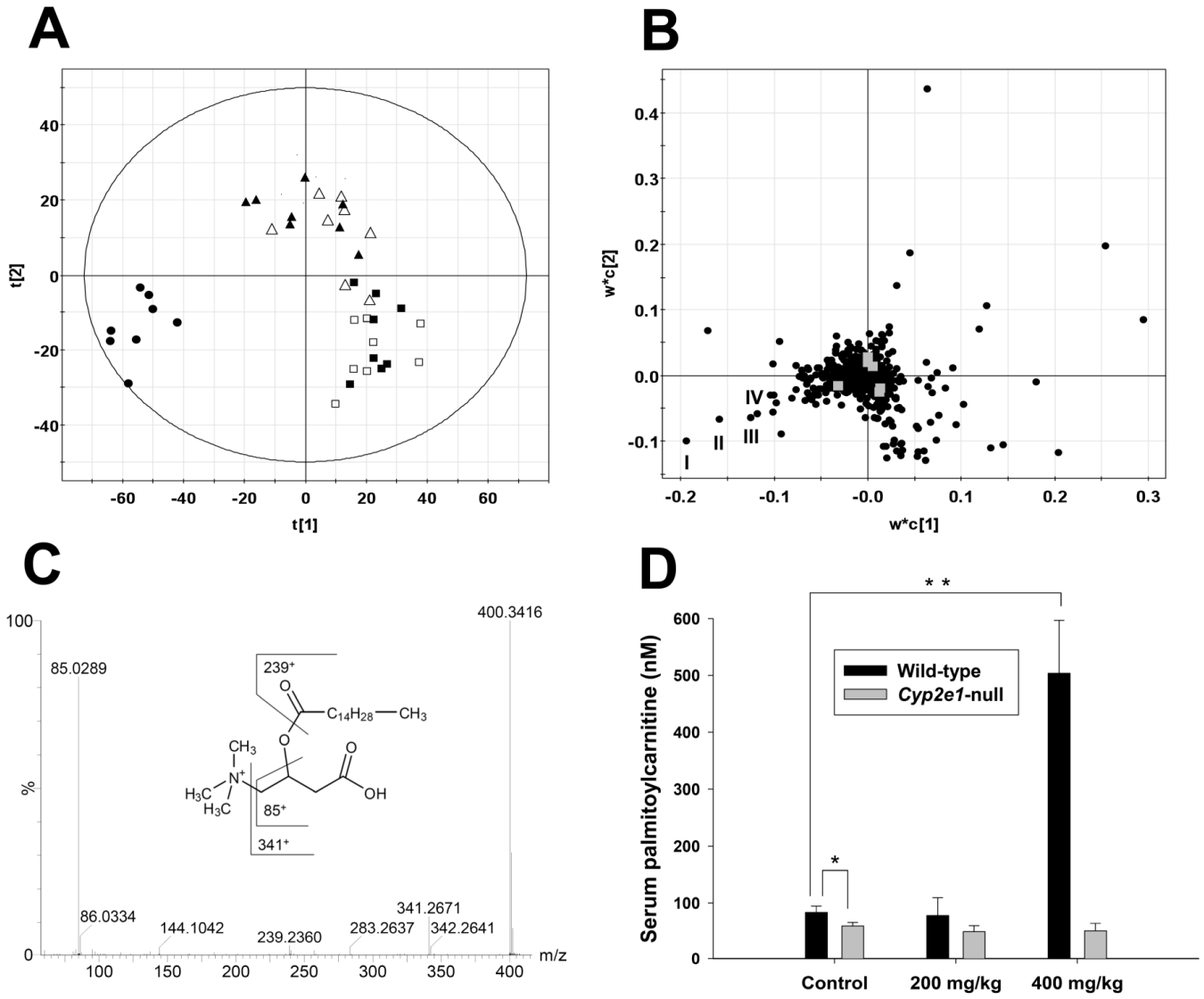

Figure 1.

Identification of acylcarnitines as serum biomarkers of APAP toxicity through metabolomic analysis of 24-h serum samples from wild-type and *Cyp2e1*-null mice treated with 200 and 400 mg/kg APAP. ***A***, Scores scatter plot of an PLS-DA model on the APAP-elicited dose-dependent influence on the serum metabolome. Details of data processing and model construction were described in the *Experimental procedures*. A two-component PLS-DA model was constructed to characterize the relationship among six mouse groups (n=7 or 8 mice/group), including wild-type mice (control: ■; 200 mg/kg APAP: ▲; 400 mg/kg APAP: •) and *Cyp2e1*-null mice (control: □; 200 mg/kg APAP: Δ; 400 mg/kg APAP: ○). The t[1] and t[2] values represent the scores of each sample in principal component 1 and 2, respectively. Fitness (R^2) and prediction power (Q^2) of this PLS-DA model are 0.486 and 0.429, respectively. The model was validated through the recalculation of R^2 and Q^2 values after the permutation of sample identities. ***B***, Loadings scatter plot representing the correlation between individual serum ion (w*) and each sample group (c) in the 1st and 2nd components of the PLS-DA model. Data points representing palmitoylcarnitine (**I**), myristoylcarnitine (**II**), oleoylcarnitine (**III**) and palmitoleoylcarnitine (**IV**) were labeled in the plot. ***C***, MS^2 fragmentation of palmitoylcarnitine (**I**). Major fragment ions were interpreted in the inlaid structural diagrams.

D, Influence of APAP treatment on serum palmitoylcarnitine level (mean ± SD) in wild-type and *Cyp2e1*-null mice (n=4; *, $p < 0.05$ and **, $p < 0.01$). Palmitoylcarnitine level in serum (mean ± SD) was measured using the multiple reactions monitoring mode in LC-MS. [$^2H_3$] palmitoylcarnitine was used as internal standard.

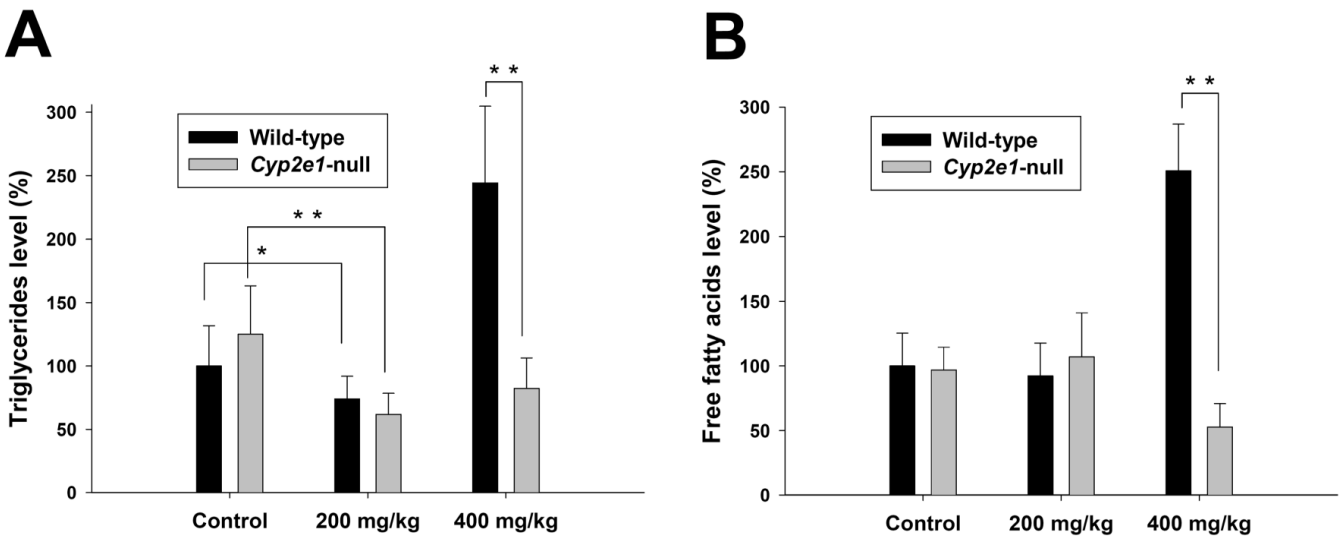

Figure 2.

Influence of APAP treatment on lipid metabolism. Triglyceride and free fatty acid levels (mean ± SD) in 24-h serum samples from wild-type and *Cyp2e1*-null mice treated with 200 and 400 mg/kg APAP were measured by colorimetric methods (n=4 mice/group; *, $p < 0.05$ and **, $p < 0.01$). ***A***, Serum triglyceride level. ***B***, Free fatty acid level. Triglyceride and free fatty acid levels in control wild-type mice were arbitrarily set as 100%.

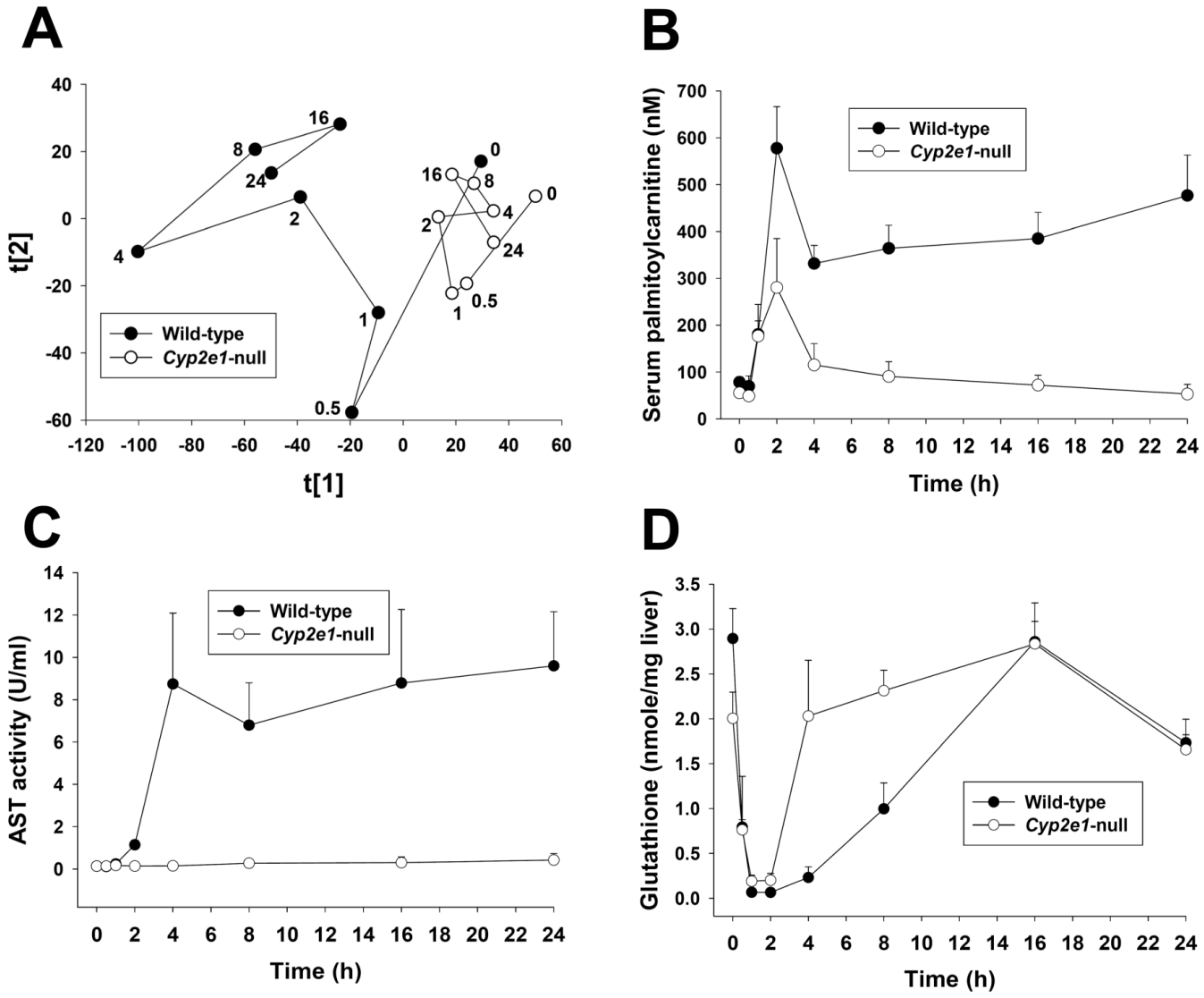

Figure 3.

Time-dependent changes in wild-type and *Cyp2e1*-null mice following 400 mg/kg APAP treatment and comparison of the biomarkers of APAP toxicity. Serum and liver samples were collected at 0, 0.5, 1, 2, 4, 8, 16, 24 h after APAP treatment. ***A***, Scores plot of PCA analysis on serum metabolomes. Details of data acquisition, processing and model construction were described in the *Experimental procedures*. Each data point represents the average of 4-8 samples in each sample group (wild-type mice: • and *Cyp2e1*-null mice: ○). The timing of sample collection was labeled beside the data point. The t[1] and t[2] values represent the scores of each sample group in principal component 1 and 2, respectively (Supplemental Figure 2A). Fitness (R^2) and prediction power (Q^2) of this PCA model are 0.388 and 0.251, respectively. ***B***, Quantitation of serum palmitoylcarnitine level in wild-type and *Cyp2e1*-null mice (mean ± SD, n=4 mice/group). Palmitoylcarnitine levels in serum was measured using the multiple reactions monitoring mode in LC-MS. [$^2H_3$]palmitoylcarnitine was used as internal standard. ***C***, Time course of AST activity in wild-type and *Cyp2e1*-null mice (mean ± SD, n=4). ***D***, Time course of hepatic glutathione level in wild-type and *Cyp2e1*-null mice (mean ± SD, n=4). Glutathione level in liver was measured using the multiple reactions monitoring mode in LC-MS.

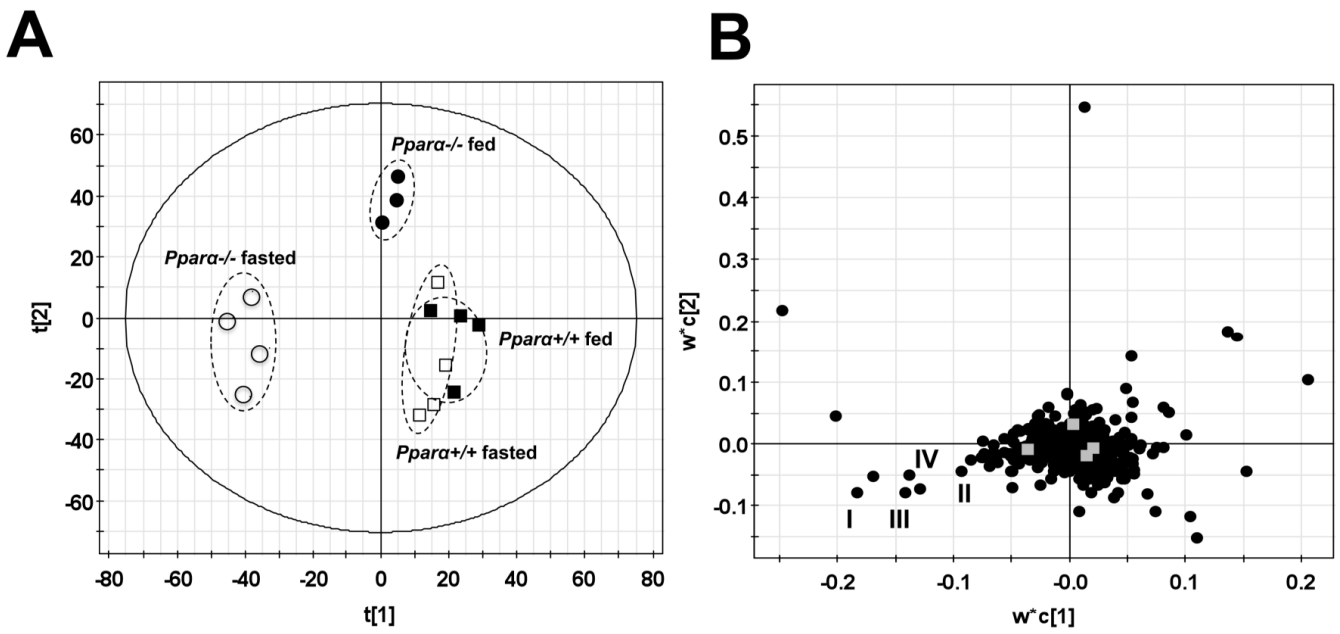

Figure 4.

Analysis of the influence of starvation on the serum metabolomes of wild-type (*Pparα*+/+) and *Pparα*-null (*Pparα*-/-) mice. ***A***, Scores scatter plot of PLS-DA model. A two-component PLS-DA model was constructed to characterize the relationship among four mouse groups (n=3 or 4 mice/group), including wild-type mice (fed: ■; fasted: □) and *Pparα*-null mice (fed: •; fasted: ○). The t[1] and t[2] values represent the scores of each sample in principal component 1 and 2, respectively. Fitness (R^2) and prediction power (Q^2) of this PLS-DA model are 0.408 and 0.25, respectively. The model was validated through the recalculation of R^2 and Q^2 values after the permutation of sample identities. ***B***. Loadings scatter plot representing the correlation between individual serum ion (w*) and each sample group (c) in the 1st and 2nd components of the PLS-DA model. Data points representing palmitoylcarnitine (**I**), myristoylcarnitine (**II**), oleoylcarnitine (**III**) and palmitoleoylcarnitine (**IV**) were labeled in the plot.

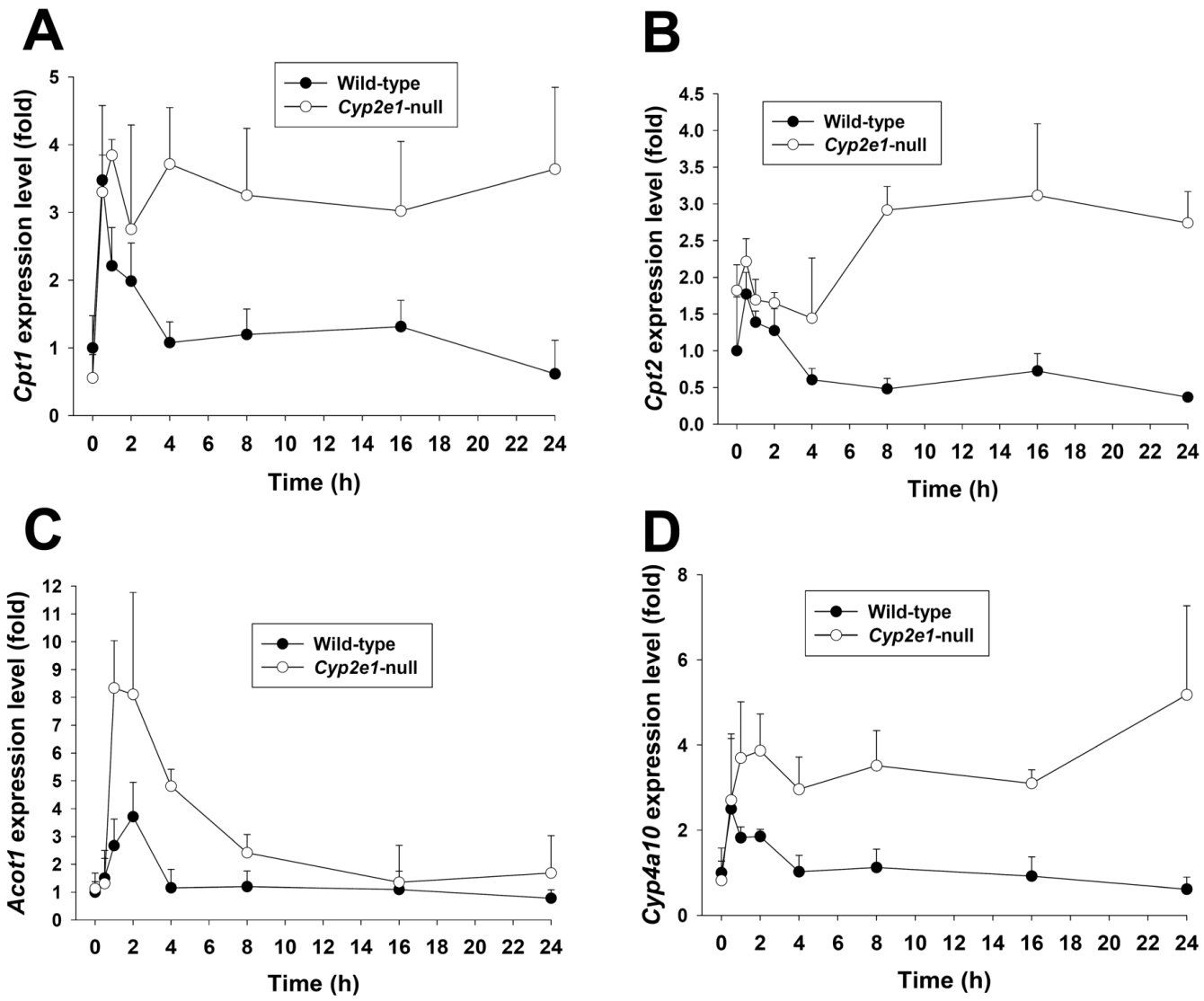

Figure 5.

Time course of *PPARα*-targeted gene expression in the livers of wild-type and *Cyp2e1*-null mice following APAP treatment. Liver samples were collected at 0, 0.5, 1, 2, 4, 8, 16, 24 h after APAP treatment (mean ± SD, n=4 mice/group). The expression levels of *PPARα*-targeted genes were measured by real-time PCR and normalized by 18S rRNA. The primer sequences are enlisted in Supplemental Table 1. ***A***, *Cpt1*. ***B***. *Cpt2*. ***C***. *Acot1*. ***D***. *Cyp4a10*. Gene expression level in control wild-type mice was arbitrarily set as 1.